33rd Annual International Conference of the IEEE EMBS
Boston, Massachusetts USA, August 30 - September 3, 2011

Topology and Conduction in the Inferior Right Atrial Isthmus Measured in Rabbit Hearts

R. Arnold, T. Wiener, D. Sanchez-Quintana, E. Hofer

Abstract—**The inferior right atrial isthmus consisting of the terminal crest, the network of pectinate muscles, and the vestibule shows very complex anatomical structure. It is seen as potential substrate for atrial flutter. In this work we present results from an electro-anatomical characterization of this region based on Cardiac Near Field recordings taken from five preparations of rabbit atrium. Pectinate muscles in the region of interest were divided into three segments: central as well as proximal and distal with respect to the terminal crest. Electrograms measured in these segments showed differences in the degree of fractionation, i.e. the numbers of distinct local activation events, indicating heterogeneities in microstructure. From 249 recording sites 63.9% showed no fractionation, 26.9% showed two activation events, and 9.2% were highly fractionated. The proximal starting sequence of activation in a series of adjacent pectinate muscles is not sorted but rather seems to be arbitrary. The same applies to the arrival sequence of activation close to the vestibule. In the network of pectinate muscles on average one proximal segment branches into two central strands and two central strands merge into one distal stem.**

I. Introduction

Atrial flutter can be caused by functional heterogeneities as well as by structural complexities of the tissue at a macroscopic and microscopic scale. Clinical electrophysiologists consider the inferior right atrial isthmus as an arrhythmogenic substrate [1]. Electro-anatomical characterization of this region of interest (ROI) based on local electrogram recordings in rabbit heart tissue is the focus of this work. Complex pathways of conduction caused by macroscopic and microscopic structures in the myocardium induce complex fractionated atrial electrograms (CFAE) at the tissue surface [2], [3]. In an earlier work we have shown that local conduction can be well described by measurements of closely spaced extracellular electrograms Φ_e and calculation of the Cardiac Near Field [4]. With flexible microminiature electrode arrays mounted on 3D-manipulators we were able to trace every branch in the network of pectinate muscles in the ROI and to reconstruct a map of local activation parameters (fractionation index FI and local activation time LAT).

Manuscript received April 15, 2011. This work was supported by the Austrian Science Fund FWF under Grant P19993-N15

R. Arnold is with the Institute of Biophysics, Medical University of Graz, Harrachgasse 21/IV, 8010 Graz, Austria (phone: +43 316 380 - 7749; e-mail: robert.arnold@medunigraz.at)

E. Hofer and T. Wiener are with the Institute of Biophysics, Medical University of Graz, Graz, Austria

D. Sanchez-Quintana is with the Department of Human Anatomy, Faculty of Medicine, University of Extremadura, Badajoz, Spain

In this work we describe and evaluate in detail the macroscopic structure and the branching topology of the pectinate muscle network in the ROI and relate the electrical parameters of conduction to the corresponding recording sites.

II. Methods and Material

A. Tissue Preparations

Rabbits were anesthetized with 5-10 mg/kg propofol and 20 µg/kg fentanyl and sacrificed according to the National Ethic Guidelines. Hearts were quickly excised and immersed in modified and oxygenated Tyrode's solution at 1-3°C. The solution contained (in mmol/l): NaCl 132.1, KCl 2.7, $CaCl_2$ 2.5, $MgCl_2$ 1.15, $NaHCO_3$ 24, NaH_2PO_4 0.42, and D-glucose 5.6. The right atrium including the intact sinus node was dissected, trimmed to the ROI and pinned down with needles on a transparent rubber carrier. Afterwards the tissue was placed in a bath and superfused with oxygenated Tyrode's solution at 36.4°C. The preparations remained autorhythmic with sinus rhythm during the whole experiment.

B. Signal Recording

Extracellular potentials Φ_e were measured with custom-designed flexible multielectrode sensors [5] capable of floating with the small displacement of the tissue during contraction. Each sensor comprises 4 quadratically arranged Ag/AgCl-electrodes with 18 µm diameter and with 50 µm interelectrode spacing. Unipolar extracellular potentials Φ_e were derived with respect to a circular Ag/AgCl reference electrode at the bottom of the tissue bath. The sensors with pre-amplifiers were mounted on micromanipulators and positioned on the tissue surface. Common procedure was to use two sensors: One was kept stationary at the proximal or distal end of a pectinate muscle and a second one was consecutively positioned along the pectinate muscle for time serial mapping of Φ_e. Tissue topology and recording sites were documented with a digital camera (Olympus C-5060 WZ, Olympus Corp., Japan). A single lead tungsten recording electrode was placed close to the sinus node to trace the sinus rhythm and to obtain a trigger source for beat-to-beat online monitoring of Φ_e. Signals were amplified by custom-designed differential amplifiers (gain 100) and lowpass filtered (-3 dB point at 20 kHz). A PXI based data acquisition system (NI PXI-6123, National Instruments, Austin, Texas) was used to digitize signals at a rate of 100 kHz per channel and 16 bit resolution.

Online monitoring and data acquisition was performed on a standard desktop PC (DELL Optiplex 755). Signal data were stored in a DADiSP compatible binary format (DSP, Newton, Massachusetts).

C. Signal Analysis

To characterize conduction along pectinate muscles the following parameters were determined: (a) fractionation index FI, (b) local activation time LAT, and (c) path length S.

FI was determined from the first temporal derivative $d\Phi_e/dt$ of the extracellular potential Φ_e. From signals with multiple negative deflections within $d\Phi_e/dt$ only those with amplitudes larger than 10% of the maximum negative deflection were taken into account as local activation event. Fractionation index FI was classified as 1 (single deflection), 2 (two independent deflections separated by at least 100 µs), and >2 (highly fractionated signals with multiple deflections).

LAT was determined as the instant of the peak negative deflection of $d\Phi_e/dt$ [6]. If FI was larger than one, LAT was determined from the largest deflection, i.e. the activation event closest to recording site.

S along the pectinate muscle was determined from digital images of the tissue preparations (see Fig. 1) and was defined as length from the origin of a pectinate muscle at the junction to the terminal crest to the corresponding recording site. The length was measured following the central longitudinal line of the pectinate muscle.

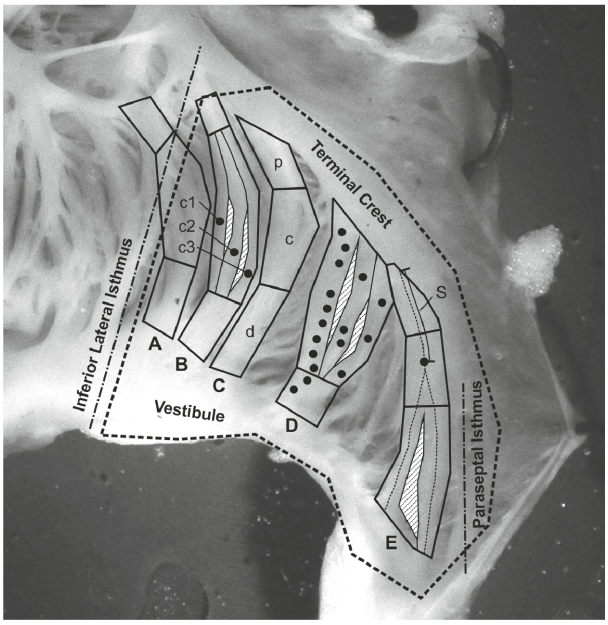

Fig. 1. Morphology and classification of tissue preparations. The region of interest ROI (dashed line) ranges from the inferior lateral isthmus to the paraseptal isthmus (dash-dotted lines). Stems of pectinate muscles PM within the ROI were labeled with uppercase letters A,B, etc. Muscles were divided into 3 segments: proximal (p), central (c), and distal (d) as shown for PM C. If branching occurred parallel segments were indexed as shown for PM B. Path length S following the central longitudinal line is indicated for PM E. For PM D recording sites are depicted.

D. Morphometry

To evaluate structural properties of the tissue preparations digital images were used. After the experiment high resolution pictures of the tissue preparation were taken using a digital SLR camera with a macro lens (Canon EOS 5D Mark II and Canon MP-E 65 mm 2.8 1-5x, Canon Inc., Japan). Pixel resolution for 1:1 images was 6.41 µm/Px and could be enhanced to 1.28 µm/Px for 5 times optically zoomed segments. Images were taken with incident light (Canon Macro Twin Lite MT-24X, Canon Inc., Japan) or with a custom-designed transillumination device.

All pectinate muscles (PM's) within the ROI were classified as follows: Each PM was divided into three segments for evaluation: proximal (p, close to the terminal crest), central (c), and distal (d, close to vestibule). Segmentation criterion was a merging or branching of major strands detected in the transillumination image of the ROI revealing fiber topology in high detail. In the vestibule (distal segment) the stems of PM's were labeled with uppercase letters A, B, C, etc. in the sequence from the inferior lateral to the paraseptal isthmus. Proceeding along the PM from the vestibule to the terminal crest the label was extended by a lowercase letter corresponding to the segment and if branching occurs with a number indexing parallel segments (e.g. Bc1, Bc2, and Bc3). Fig. 1 illustrates this classification.

III. Results

All values are given in mean ± standard deviation.

Data from five experiments were analyzed. The basic cycle length at sinus rhythm was 373±42 ms (see Table 1).

In the tissue preparations between 3 and 5 pectinate muscles were identified. PM's with sufficient recording sites

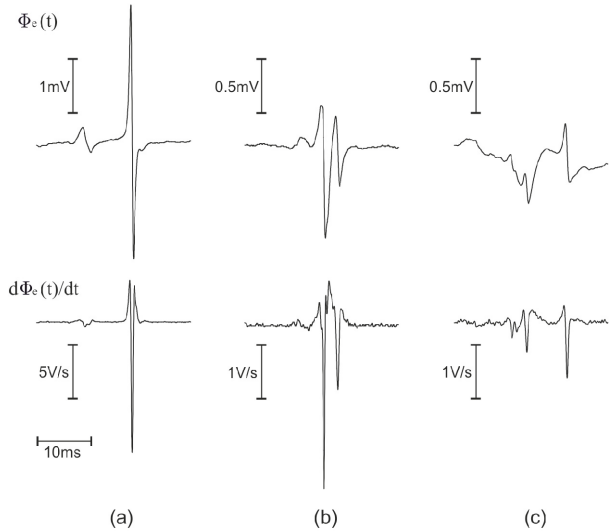

Fig. 2. Examples of extracellular potentials $\Phi_e(t)$ (top row) and respective temporal derivatives $d\Phi_e/dt$ (bottom row) with different fractionation index FI. (a) FI=1 suggests well coupled and parallel oriented fibers. The first small biphasic deflection in $\Phi(t)$ reveals a distant and not a local depolarization. (b) Fractionated electrogram with FI=2 showing two independent deflections in its derivative. (c) Highly fractionated electrogram.

TABLE I
RESULTS OF 5 ATRIAL PREPARATIONS

Atrium	BCL	Sites[a]	Fractionation Index FI			CV[b]	Number of Segments			Diameter (mm)		
	(ms)		1	2	>2	(m/s)	prox	cent	dist	prox	cent	dist
1	365±25	50	32 (64.0%)	16 (32.0%)	2 (4.0%)	0.79±0.28	3	9	3	1.50±0.89	0.61±0.14	1.37±0.21
2	358±3	42	26 (61.9%)	14 (33.3%)	2 (4.8%)	0.89±0.38	5	12	6	0.90±0.34	0.59±0.32	1.09±0.32
3	389±43	34	16 (47.1%)	9 (26.5%)	9 (26.5%)	0.52±0.85*	9	8	4	0.56±0.29	0.46±0.13	0.77±0.12
4	428±52	42	25 (59.5%)	7 (16.7%)	10 (23.8%)	0.79±0.28	4	7	5	0.93±0.42	0.75±0.40	1.07±0.35
5	353±30	81	60 (74.1%)	21 (25.9%)	-	0.74±0.27	4	7	5	0.97±0.36	1.16±0.63	1.29±1.08
Sum	**373±42**	**249**	**159 (63.9%)**	**67 (26.9%)**	**23 (9.2%)**	**0.74±0.48**	**25**	**43**	**23**	**0.86±0.49**	**0.69±0.41**	**1.11±0.55**

Values are mean ± standard deviation
BCL…basic cycle length, CV…conduction velocity, prox…proximal, cent…central, dist…distal
[a] number of recording sites. [b] estimated by linear regression for all recording sites along a pectinate muscle.
* high standard deviation due to retrograde conduction in three individual central segments

(≥5) were included into analysis leading to a total of 249 recording sites. 63.9% of the sites showed no fractionation (FI=1), 26.9% FI=2, and 9.2% highly fractionated signals (FI>2). Table 1 shows the distribution of FI in more detail.

A. Fractionation along Pectinate Muscles

Highly fractionated signals with FI>2 were more often observed in the proximal segments (20.5%). This percentage decreased to 7.7% in the central segments and to 4.8% in the distal segments. On the other hand non-fractionated signals (FI=1) increased from 59.1% proximal to 62.0% central and to 71.4% distal. Signals with FI=2 were measured most often in the central segments (30.3%) and almost equally proximal and distal (20.5% proximal and 23.8% distal). Fig. 2 illustrates signals with different FI.

B. Activation along Pectinate Muscles

Conduction along PM's in the ROI was investigated by examining LAT and S for each strand by creating time-distance diagrams. The mean conduction velocity in the PM was estimated by linear regression. This was done in two steps: (i) only recording sites with FI=1 were included since LAT is uniquely evaluable and (ii) all recording sites were included with LAT determined for the most dominant deflection in signals with FI>1. Fig. 3 shows two exemplary linear fits. The overall conduction velocity was 0.68±0.59 m/s for signals with FI=1 and 0.74±0.48 m/s for all recording sites.

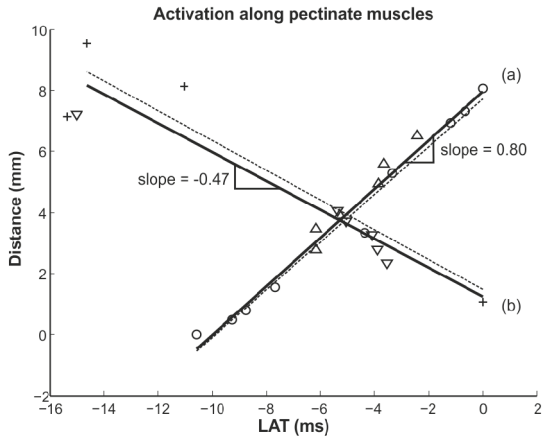

Fig. 3. Activation along pectinate muscles. Linear regression was performed for recording sites with FI=1 (+ and o) and for FI≥2 (△ and ▽). Solid lines show results for FI=1 and dashed lines results for FI≥2. Pectinate muscle (a) is activated antegrade (positive slope) with a conduction velocity of CV=0.80 m/s. Pectinate muscle (b) is activated retrograde (negative slope) with CV=0.47 m/s.

In one experiment three PM's showed retrograde conduction in the central segment at sinus rhythm. Fig. 3 illustrates the time-distance diagram of one of these strands.

C. Activation Sequence of Pectinate Muscles

The sequence in which the PM's were activated was determined from the LAT of the recording site closest to the terminal crest. The sequence indices of starting activation showed that it was not sorted from left to right i.e. from sinus node to the paraseptal isthmus as expected (cp. Figure 1). It rather was arbitrary and so was the arrival sequence in the vestibule. Furthermore the two sequences did not correspond to each other. Fig. 4 illustrates this finding for one experiment.

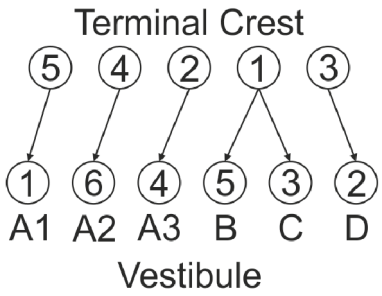

Fig. 4. Start and arrival sequence in the ROI. Start sequence and arrival sequence did not correspond. Note that stem A in the vestibule had a large diameter and therefore three distinct LAT's were evaluated.

D. Morphometric Evaluation

We found between 3 and 9 proximal segments in the five preparations. They split up into 7 to 12 central segments and merged into 3 to 6 distal stems. On average a PM splits up from one proximal segment into two central strands and two strands merge into one distal stem (overall 25 proximal, 43 central, and 23 distal).

Proximal segments had a diameter of 0.86±0.49 mm, the central segments were the thinnest with 0.69±0.41 mm diameter, and the distal stems were the largest structures with 1.11±0.55 mm diameter.

IV. Discussion

The network of PM's in the ROI is manifold in its structure and topology. In direction from the inferior lateral isthmus to the paraseptal isthmus the number of strands changes by branching and merging of fibers. The central segment of PM's shows the largest number of fiber bundles (7 to 12), the distal segment the smallest one (3 to 6) since the PM's merge to thick and stem like tissue structures entering the vestibule. Such complex and inter-individual diverse topologies of conducting structures have an impact on heterogeneity of local excitation spread. We have tried to schematize this structure by choosing an appropriate notation.

Electrograms show uniform non-fractionated, fractionated, and highly fractionated waveforms within each muscle and even within one individual segment. Uniform electrograms indicate well coupled and parallel oriented fibers in the vicinity of the recording sites (~500 µm). Fractionated electrograms are expected at branching or merging muscles or if two adjacent but electrically uncoupled fibers run in parallel and the activation wavefronts are delayed to each other. Highly fractionated electrograms indicate either a large number of branches or multiple and sudden changes of fiber directions where transition from longitudinal to transverse conduction occurs.

The distal segments show the highest percentage of uniform electrograms, indicating well coupled parallel organization of the fibers merging in the thick and stem like structures. The highest percentage of FI=2 can be found in the central segments, indicating frequent occurrence of adjacent strands. Electrograms with FI>2 are most found in the proximal segments representing the initiation of activation leaving the terminal crest and entering the individual PM strands. This might result from heterogeneity of activation due to complex micro- and macrostructure. Highly fractionated electrograms with time intervals of less than 0.5 ms between the individual deflections of $d\Phi_e/dt$ and low amplitudes probably indicate crossing fibers or local patchy fibrosis. Results of computer simulations based on digitized histographs of atrial tissue confirm this assumption [7].

Determination of LAT from the largest deflection of $d\Phi_e/dt$ when FI is larger than 1 is appropriate only if equal distribution of current source densities and equal upstroke velocities in the tissue are assumed. This holds for the tissue preparations used in this work but might be different in preparations comprising the Purkinje network or very large current sources which could induce large deflections in $d\Phi_e/dt$ although they are not the sources closest to the recording site.

We found that the spatial sequence of local activation along the terminal crest and the vestibule does not correspond, nor is it always monotone. The arrival sequence in the vestibule depends on the starting sequence close to the terminal crest, the length of the PM, and the corresponding mean conduction velocity along the PM. However, the non-monotone starting sequence probably caused by complex conduction in the terminal crest as well as heterogeneous transition processes between terminal crest and PM has to be further investigated (effects of high anisotropy ratio [8]). Additionally a quantitative measure has to be found to describe the degree of disorganization. This could be done by calculating a mean squared error between starting and arrival sequence. Open question is how to deal with branching and merging fibers and with inter-pectinate conduction pathways.

We also found in single experiments that individual PM's run retrograde excitation spread even during normal sinus rhythm, a fact that would allow possible macroscopic reentry circuits. Possible reasons for retrograde conduction might be a conduction block at the junction between terminal crest and PM's or bypassing epicardial conduction pathways.

A. Limitations:

The measurements done here were restricted to the dominant endocardiac structures in the ROI. Very thin muscle fiber networks (diameter < 0.3 mm) between the pectinate muscles are rather part of the epicardiac network of connective tissue and extremely thin strands. They are difficult to indentify optically and electrically during the experiment. The strength of their current sources is considered to be negligible compared to the large pectinate muscles. However, we found that the very thin epicardial network of strands sometimes differs in direction from that of the endocardiac strands which opens the hypothesis that endocardiac and epicardiac activation could differ – an additional possible factor of atrial arrhythmogenesis.

References

[1] J.A. Cabrera, D. Sanchez-Quintana, J. Farre, J.M. Rubio and S.Y. Ho, "The inferior right atrial isthmus: Further architectural insights for current and coming ablation technologies", *J Cardiovasc Electrophysiol*, vol. 16, pp. 402-408, April 2005

[2] V. Jacquemet, C.S. Henriquez, "Genesis of complex fractionated atrial electrograms in zones of slow conduction: A computer model of microfibrosis", *Heart Rhythm*, vol. 6, pp. 803-810, 2009

[3] J.M.T. de Bakker, F.H.M. Wittkampf, "The pathophysiologic basis of fractionated and complex electrograms and the impact of recording techniques on their detection and interpretation", *Circ Arrhythm Electrophysiol.*, vol. 3, pp. 204-213, 2010

[4] E. Hofer, T. Wiener, F. Keplinger, P. Svasek, D. Sanchez-Quintana, V. Climent, A. Lueger, G. Plank, „Cardiac near field sensors – Technical requirements and validation procedures", *IFMBE Proc.*, Prague, Czech Republic, 2005

[5] E. Hofer, F. Keplinger, T. Thurner, T. Wiener, D. Sanchez-Quintana, V. Climent, G. Plank, "A new floating sensor array to detect electric near fields of beating heart preparations", *Biosensors and Bioelectronics*, vol. 21, pp. 2232-2239, 2006

[6] M.S. Spach, J.M. Kootsey, "Relating the sodium current and conductance to the shape of transmembrane and extracellular potentials by simulation: Effects of propagation", *IEEE JBME*, vol. 32, pp. 743-755, 1985

[7] F.O. Campos, T. Wiener, H. Ahammer, G. Plank, R. Weber Dos Santos, D. Sanchez-Quintana, E. Hofer, „A 2D-computer model of atrial tissue based on histographs describes the electro-anatomical impact of microstructure on endocardiac potentials and electric near-fields", *ConfProc IEEE Eng Med Biol Soc*, pp. 2541-2544, 2010

[8] A.G. Kleber, Y. Rudy, "Basic mechanisms of cardiac impulse propagation and associated arrhythmias", *Physiol Rev*, vol. 84, pp. 431-488, 2004